*Journal of Machine Engineering, 2026, Vol. 26,*
*ISSN 1895-7595 (Print)  ISSN 2391-8071 (Online)*

Received*: 30 January 2026* / Accepted: *10 March 2026* / Published online: *16 April 2026*

*thickness uniformity, finite element modeling,*
*hydraulically assisted incremental forming,*
*AA1050 aluminum alloy*

Thanh -Huan NGUYEN[1], The -Thanh LUYEN[2],
Duc -Toan NGUYEN[3*]

# HYDRAULICALLY ASSISTED SINGLE POINT INCREMENTAL FORMING OF AA1050 ALUMINUM: EXPERIMENTAL–NUMERICAL ANALYSIS OF WALL THICKNESS IN TRUNCATED QUADRILATERAL COMPONENTS

This study reports a combined experimental–numerical investigation of hydraulic-assisted single point incremental forming (HA-SPIF) to enhance thickness uniformity in truncated quadrilateral parts formed from AA1050 aluminum alloy sheets. A finite element model is established and validated using experiments on circular blanks of 220 mm diameter and 1.0 mm thickness, forming components with a 60° wall angle and a target height of 55 mm. Material anisotropy is characterized through uniaxial tensile tests along 0°, 45°, and 90° to the rolling direction, and direction-dependent Voce hardening laws are calibrated from true stress–strain data, with flow stresses of 69.0–82.6 MPa and anisotropy coefficients of 0.45–0.86. The validated model is first employed to assess the effect of material orientation on thickness distribution, revealing pronounced differences in thinning behaviour. A subsequent parametric study examines the coupled influences of hydraulic pressure, tool feed rate, and vertical step size on thickness variation and minimum residual thickness. Hydraulic assistance is shown to effectively suppress localized thinning and significantly improve thickness homogeneity relative to conventional SPIF. The main contribution of this work is the integrated consideration of anisotropic Voce hardening and hydraulic support for a non-axisymmetric geometry, providing a reliable predictive framework and practical guidelines for thinning control in high-precision forming applications.

## 1. INTRODUCTION

Single Point Incremental Forming (SPIF) has emerged as a highly flexible and cost-effective sheet metal forming technique, particularly suited for rapid prototyping and small-batch production. By employing a numerically controlled hemispherical tool to progressively deform a clamped sheet without the need for dedicated dies, SPIF enables the fabrication of complex three-dimensional geometries with minimal tooling investment. The process can be readily implemented on conventional CNC milling machines, industrial robots, or customized

[1] Faculty of Mechanical Engineering, University of Economics – Technology for Industries, Vietnam
[2] Faculty of Mechanical Engineering, Hungyen University of Technology and Education, Vietnam
[3] School of Mechanical Engineering, Hanoi University of Science and Technology, Vietnam
[*] E-mail: toan.nguyenduc@hust.edu.vn
https://doi.org/10.36897/jme/219077

forming platforms, making it accessible to both academic research and industrial practice. Owing to this flexibility, a thorough understanding of forming forces and deformation mechanisms is essential to ensure machine safety, optimize tool selection, and prevent excessive loading, all of which directly influence formability, surface integrity, and tool wear [1], [2], [3–5]. Consequently, reducing forming forces while maintaining acceptable surface quality remains a central technical challenge in SPIF, commonly addressed through process parameter optimization, thermal assistance, and advanced toolpath design strategies.

The localized plastic deformation inherent to SPIF is governed by a wide range of interacting factors, including machine-related parameters, process parameters, and workpiece characteristics [1]. Among workpiece-related factors, both material properties and part geometry play decisive roles. In particular, the wall angle α is widely recognized as a critical geometric parameter that strongly governs the achievable forming depth and the onset of fracture. An increase in wall angle generally leads to higher strain localization and accelerated thinning, thereby limiting formability and dimensional accuracy [2]. As a result, controlling thickness distribution and suppressing excessive thinning remain key obstacles, especially for components with steep walls or non-axisymmetric geometries.

To further enhance the forming limits and dimensional stability of SPIF, considerable research effort has been devoted to integrating auxiliary physical fields, such as elevated temperature, ultrasonic vibration, and hydraulic pressure. Among these approaches, the incorporation of hydraulic pressure has demonstrated particular promise. This hybrid process, commonly referred to as HA-SPIF, employs pressurized fluid beneath the sheet to act as a compliant and adaptive support during deformation. The hydraulic medium effectively functions as a flexible die, modifying the stress state in the deformation zone, reducing springback, and improving geometric accuracy and thickness distribution [3]. In HA-SPIF, hydraulic pressure becomes a key control variable, directly influencing material flow, strain paths, and the onset of localized thinning.

Several studies have explored the influence of hydraulic assistance on SPIF performance. Ali Abdelhafeez Hassan et al. [4] investigated the combined effects of hydraulic pressure and wall angle on the forming height of dual-phase DP600 steel sheets, considering pressure levels of 0, 0.2 bar, and 0.4 bar. Their results indicated a substantial increase in achievable forming height with decreasing wall angle, with successful forming at a wall angle of 65° under hydraulic assistance. Afshin Fatemi et al. [5] proposed the HA-SPIF process as a novel route to improve formability, demonstrating through experiments and finite element (FE) simulations that forming limits under non-planar stress states decrease progressively from plane strain to biaxial tension. Miao Shang et al. [6] systematically analysed the effects of hydraulic parameters on thickness distribution and critical wall angle in HA-SPIF of truncated pyramid geometries, reporting a non-monotonic influence of pressure: increasing pressure initially raises the minimum wall thickness, followed by a reduction at higher pressure levels. In parallel, numerous experimental and numerical studies have focused on conventional SPIF of truncated cone geometries fabricated from AA1050 aluminum alloy, examining the roles of process parameters and wall angle on forming height and thickness evolution [7–11].

Despite these advances, several limitations remain evident in the current literature. First, most existing HA-SPIF studies concentrate on axisymmetric or relatively simple geometries,

whereas non-axisymmetric shapes, such as truncated quadrilateral components, are less explored despite their practical relevance. Second, the majority of numerical investigations adopt isotropic or simplified material models, neglecting the pronounced anisotropy introduced by rolling in aluminum sheets. This simplification can lead to inaccurate predictions of thickness distribution and localized thinning, particularly when material flow is direction-dependent. Third, the coupled effects of hydraulic pressure and material anisotropy on thickness uniformity have not yet been systematically addressed within a unified experimental–numerical framework.

In response to these gaps, the present study develops an integrated experimental and finite element modeling framework for HA-SPIF of truncated quadrilateral components fabricated from AA1050 aluminum alloy. A key originality of this work lies in the explicit incorporation of direction-dependent Voce hardening laws calibrated along three material orientations (0°, 45°, and 90° relative to the rolling direction) to rigorously assess their influence on thickness uniformity. The numerical model is first validated against experimental measurements to identify the hardening orientation that best reproduces the observed thickness distribution. Subsequently, the validated framework is employed to conduct a comprehensive parametric study on the effects of hydraulic pressure, tool feed rate, and vertical step size on wall thinning and thickness homogeneity. By ensuring that all simulation parameters are directly verifiable through experiments, the proposed approach enhances the reliability and predictive capability of HA-SPIF models. Overall, this study not only advances the fundamental understanding of anisotropy-aware HA-SPIF for non-axisymmetric geometries but also provides practical guidelines for thinning mitigation in high-precision applications, including aerospace structures, biomedical components, and customized lightweight products.

## 2. PRODUCT GEOMETRY AND MATERIAL MODELING

The present investigation was conducted using commercially pure aluminum alloy AA1050, a material widely employed in key industrial sectors such as food processing and packaging, chemical equipment, architecture, and decorative and artistic applications [12]. Owing to its excellent corrosion resistance, high ductility, and superior formability, AA1050 is particularly suitable for manufacturing thin-walled components with complex geometries. These attributes make it an ideal candidate for SPIF, especially in applications where frequent design changes, geometric complexity, and low production volumes render conventional die-based forming economically inefficient.

The target component in this study is a truncated quadrilateral geometry, selected deliberately to represent a non-axisymmetric shape that poses greater challenges in terms of thickness uniformity and strain localization compared with commonly studied axisymmetric forms. The experimental blank was a circular AA1050 sheet with a diameter of 220 mm and an initial thickness $t_0$ = 0.5 mm. The final formed geometry consisted of a truncated quadrilateral pyramid with a forming height of $H$ = 55 mm and a constant wall angle of $\alpha$ = 60º, as illustrated in Fig. 1. This geometry was chosen to intensify non-uniform material flow along different edges and corners, thereby providing a rigorous test case for assessing

the predictive capability of anisotropy-aware HS-SPIF simulations component considered in the HA-SPIF study, including the initial blank size, forming height $H$ = 55 mm, wall angle $\alpha$ = 60º, and reference directions used for thickness evaluation. In incremental forming processes, material anisotropy induced by rolling plays a critical role in governing deformation paths, thickness evolution, and the onset of localized thinning. Neglecting this anisotropy can lead to substantial discrepancies between numerical predictions and experimental observations, particularly for non-axisymmetric components. To accurately characterize the anisotropic mechanical behaviour of AA1050, uniaxial tensile specimens were prepared along three material orientations: the rolling direction (RD, 0°), the transverse direction (TD, 90°), and at 45° relative to RD. All tensile tests were performed using a YS-L45-J11 universal testing machine in accordance with ISO 6892-1, ensuring consistency and repeatability of the measured data.

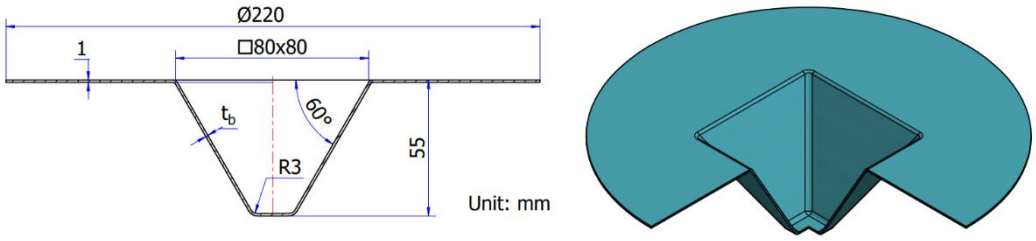


Fig. 1. Geometric configuration and principal dimensions of the truncated quadrilateral

The experimentally obtained mechanical properties are summarized in Table 1. The results reveal a clear directional dependence of yield strength and plastic anisotropy, with yield stresses ranging from 69.02 MPa to 82.64 MPa and Lankford coefficients *rrr* varying between 0.45 and 0.86. Such variations confirm the pronounced anisotropic nature of AA1050 sheets and underscore the necessity of incorporating direction-dependent material descriptions in numerical simulations of SPIF and HS-SPIF processes. The elastic modulus, density, and Poisson's ratio were assumed to be isotropic and were taken as 69 kN/mm², $2.7\times10-6$ kg/mm³, and 0.33, respectively.

Table 1. Direction-dependent mechanical properties of the AA1050 aluminium alloy obtained from uniaxial tensile tests conducted along the rolling direction (RD), 45° to RD, and transverse direction (TD)

| Mechanical property | 0° (RD) | 45° to RD | 90° (TD) |
|---|---|---|---|
| Yield strength, $\sigma_Y$ (MPa) | 82.64 | 69.02 | 76.85 |
| Lankford coefficient, r | 0.78 | 0.45 | 0.86 |
| Elastic modulus, E (kN/mm²) | - | 69 | - |
| Density, ρ (kg/mm³) | - | $2.7 \times 10^{-6}$ | - |
| Poisson's ratio, ν | - | 0.33 | - |

To capture the strain hardening behaviour of AA1050 with sufficient fidelity, true stress–true strain curves obtained from the tensile tests were used to calibrate a Voce hardening model along each material orientation. The Voce constitutive relationship is expressed as:

$$\overline{\sigma} = \sigma_Y + P(1 - exp(-Q\overline{\varepsilon})) \tag{1}$$

where $\sigma$ and $\overline{\varepsilon}$ denote the equivalent true stress and equivalent true strain, respectively, $\sigma_Y$ is the initial yield stress, and $P$ and $Q$ are material-dependent hardening parameters. The calibrated Voce parameters for AA1050 were determined separately for each orientation: for RD (0°), $\sigma_Y$=84.64 MPa, $P$ = 17.26, and $Q$ =16.18; for 45° to RD, $\sigma_Y$ =69.02 MPa, $P$=38.51, and $P$=12.65; and for TD (90°), $\sigma_Y$ = 76.85 MPa $P$ = 32.04, and $Q$ =15.06.

Figure 2 compares the experimentally measured true stress–strain curves with the corresponding Voce model fits for all three orientations. An excellent agreement is observed across the full plastic strain range, indicating that the Voce model accurately reproduces the anisotropic hardening behaviour of AA1050. This level of agreement is essential for reliable numerical prediction of thickness distribution and thinning in HA-SPIF, where localized strains can be substantial and highly direction-dependent.

The originality of the present approach lies in the explicit integration of direction-dependent Voce hardening into the HS-SPIF simulation of a truncated quadrilateral geometry. By coupling detailed experimental characterization with anisotropy-aware constitutive modelling, the proposed framework avoids oversimplified isotropic assumptions and significantly enhances the predictive accuracy of SPIF simulations. This material modelling strategy forms a robust foundation for the subsequent numerical analyses of hydraulic pressure, tool feed rate, and step size effects on thickness uniformity and thinning behaviour.

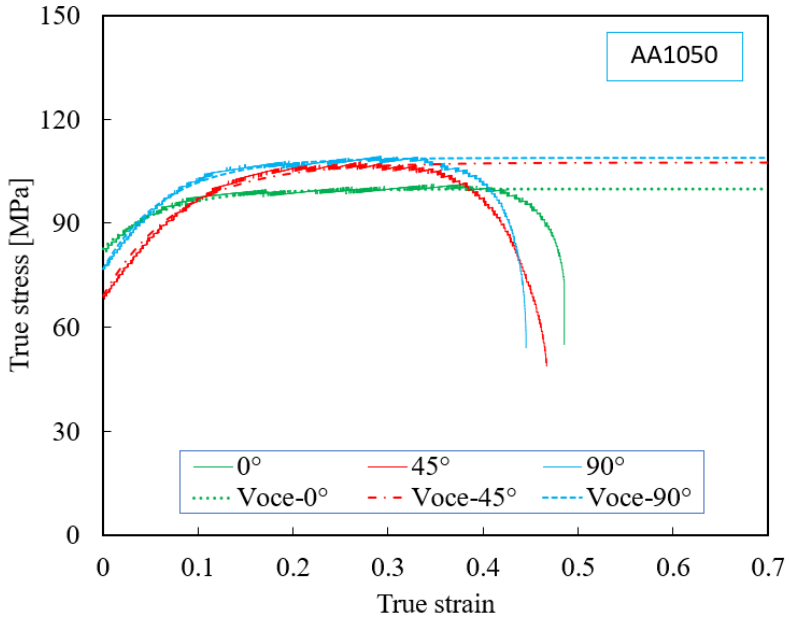


Fig. 2. Comparison between experimentally obtained true stress–strain curves and the corresponding Voce hardening model fits for AA1050 aluminum alloy along the rolling direction (0°), 45° to the rolling direction, and the transverse direction (90°), highlighting the anisotropic plastic response of the material

# 3. NUMERICAL AND EXPERIMENTAL METHODOLOGY

## 3.1 FINITE ELEMENT SIMULATION MODEL

A three-dimensional FE model was developed to simulate the HA-SPIF process using Abaqus/Explicit 6.13 [13]. The model explicitly represents the interaction between the AA1050 aluminum sheet, the forming tool, the supporting die, and the clamping system, as illustrated in Figure 3a. The aluminum sheet was discretized using reduced-integration shell elements (S4R), which are well suited for large plastic deformation and contact-dominated forming processes, while the forming tool, backing plate, and fixture components were modelled as rigid bodies to reduce computational cost without compromising accuracy.

A distinctive feature of the present simulation framework is the explicit incorporation of hydraulic pressure acting on the lower surface of the sheet, representing the flexible hydraulic medium confined within a sealed cavity (Fig. 3b). This reverse pressure provides adaptive support during deformation and fundamentally alters the local stress state compared with conventional SPIF. The pressure loading was applied uniformly and maintained throughout the forming process to replicate experimental conditions. The final deformed geometry obtained from the numerical simulation is shown in Fig. 3c.

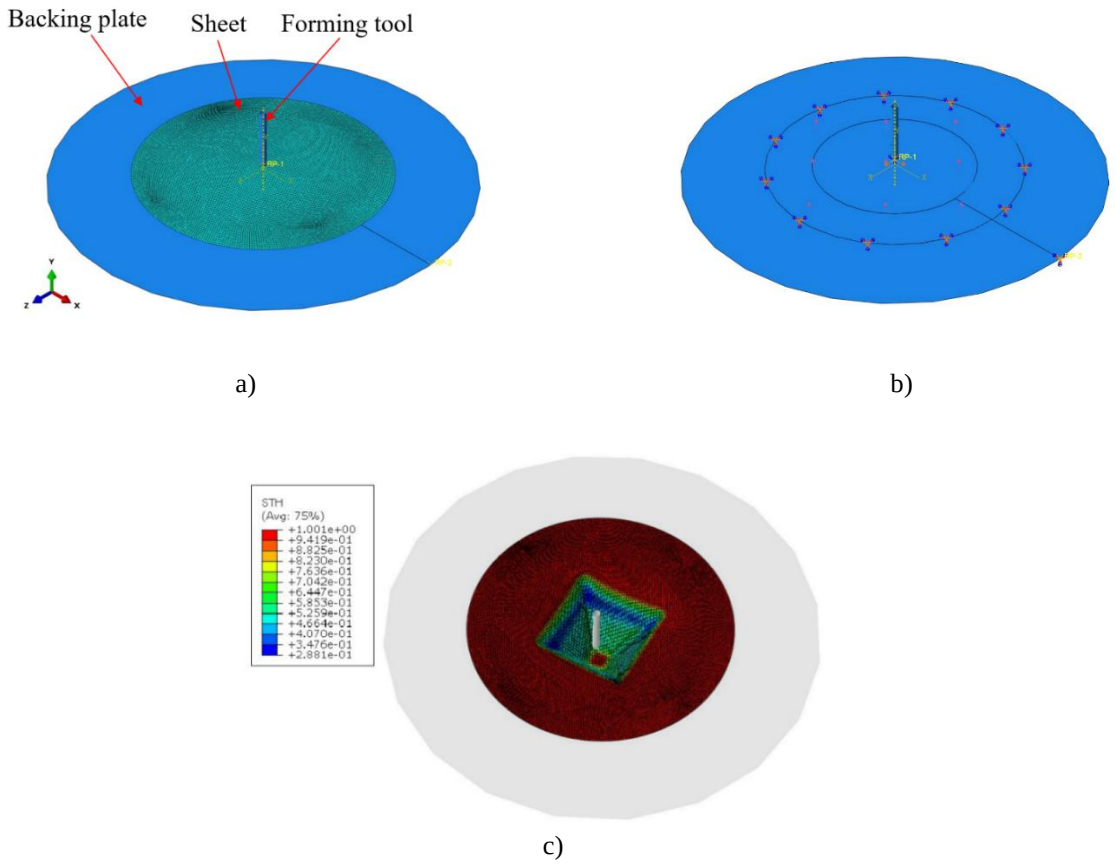


Fig. 3. a) Finite element model of the HA-SPIF process; b) schematic illustration of hydraulic pressure applied to the lower surface of the sheet; c) numerically predicted final geometry after forming

Tool motion was defined through a spiral toolpath generated directly from NC G-code, extracted using G-Code Ripper software, ensuring strict consistency between numerical and experimental setups (Fig. 4). The forming tool followed a prescribed vertical incremental trajectory with a constant step-down, while the in-plane motion was controlled to maintain a continuous contact condition. Contact interactions were modeled using an isotropic Coulomb friction law. The friction coefficient between the forming tool and the sheet was set to $\mu$ = 0.05. This value was established through preliminary calibration tests performed under the same lubrication conditions as the experiments (mineral oil lubrication). A sensitivity analysis was conducted within the range $\mu$ = 0.03–0.08 to assess its influence on forming force response and wall thickness distribution. Among the evaluated values, $\mu$ = 0.05 provided the closest agreement between numerical predictions and experimental measurements in terms of both forming forces and thickness profiles. Accordingly, this calibrated value was adopted in all subsequent simulations. A fully constrained contact condition was imposed between the sheet, backing plate, and fixture, consistent with previously reported HA-SPIF modelling approaches [5].

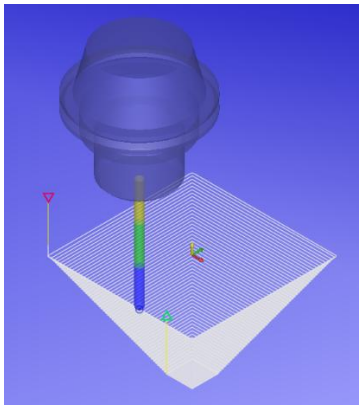

a)

```
O0000(A60_V1_TZ1)
N100 G21
N102 G0 G17 G40 G49 G80 G90
N104 T240 M6
N106 G0 G90 G54 X-38.101 Y-38.107 S2400 M3
N108 Z25.
N110 Z4.5
N112 G1 Z-.5 F1000.
N114 X-37.982 Y-38.204
N116 X-37.83 Y-38.279
N118 X-37.638 Y-38.33
N120 X-37.314 Y-38.355
N122 X37.303
N124 X37.649 Y-38.327
N126 X37.838 Y-38.277
N128 X37.988 Y-38.202
N130 X38.099 Y-38.112
N132 X38.206 Y-37.979
N134 X38.279 Y-37.831
N136 X38.329 Y-37.641
N138 X38.355 Y-37.313
N140 Y37.316
N142 X38.328 Y37.647
N144 X38.281 Y37.825
N146 X38.201 Y37.983
N148 X38.095 Y38.114
N150 X38.012 Y38.182
N152 X37.965 Y38.215
N154 X37.838 Y38.277
```

b)

Fig. 4. a) Spiral toolpath employed in the numerical simulation; b) corresponding NC G-code used for experimental implementation

Material behaviour was modeled by combining elastic–plastic constitutive laws with anisotropic hardening effects. Density, Young's modulus, and Poisson's ratio were taken as isotropic, while plastic deformation was governed by direction-dependent Voce hardening laws calibrated from uniaxial tensile tests conducted along 0°, 45°, and 90° relative to the rolling direction. This modeling strategy represents a key novelty of the present work, as it enables the FE model to capture both the anisotropic response of AA1050 and the stress redistribution induced by hydraulic support, thereby significantly improving the reliability of thickness prediction in non-axisymmetric geometries.

### 3.2. EXPERIMENTAL SETUP

The HS-SPIF experimental fixture was specifically designed and manufactured to validate the numerical model, as shown in Figure 5a. The fixture consists of a sealed forming

chamber and a clamping plate. The chamber body was welded to ensure hydraulic tightness and filled with hydraulic oil, while the clamping plate was used to rigidly fix the blank during forming. This configuration allows the hydraulic medium to act as a compliant die, providing continuous support against local thinning.

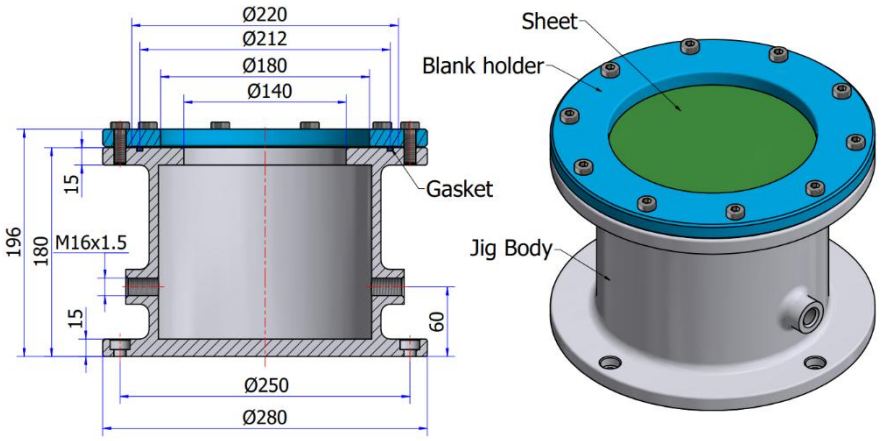


a)

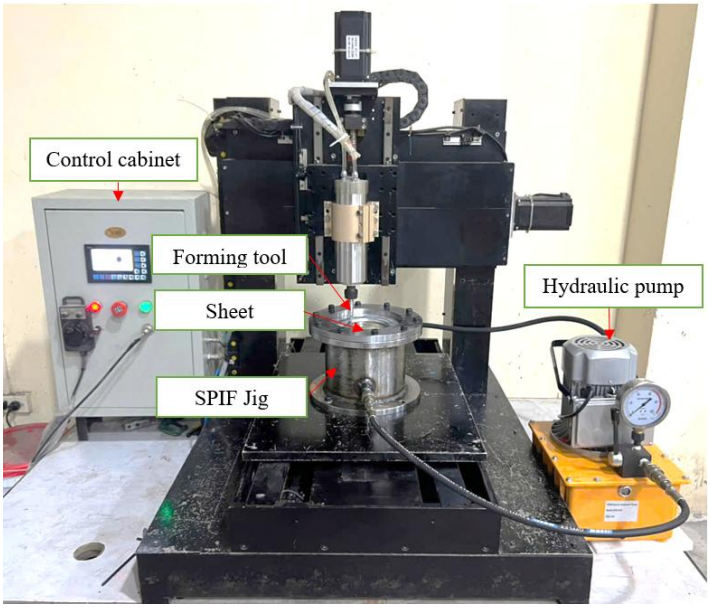


b)

Fig. 5. a) Geometry and structural layout of the custom-designed HA-SPIF fixture, illustrating the sealed hydraulic chamber and clamping system; b) experimental HA-SPIF setup, showing the three-axis CNC milling machine integrated with the hydraulic support fixture used in the forming trials

All experiments were carried out on a three-axis CNC milling machine with a working envelope of 500 × 500 × 350 mm, a maximum spindle speed of 12,000 rpm, and a spindle power of 2.5 kW (Fig. 5b). The HA-SPIF fixture was rigidly bolted to the machine table, and the sheet blank was clamped between the backing plate and the fixture body using M10 bolts to prevent slipping and unintended deformation. Structural components of the fixture were manufactured from C45 steel to ensure sufficient stiffness under hydraulic loading.

The forming tool featured a hemispherical tip with a diameter of 6 mm and was fabricated from heat-treated SKD11 tool steel with a hardness of approximately 55 HRC. The surface roughness at the tool tip was controlled to $Ra \approx 0.25$ μm to minimize frictional effects. VG68 lubricating oil was applied to further reduce tool–sheet friction and stabilize forming conditions. Hydraulic pressure was supplied by an electrically driven pump connected to the fixture through inlet and outlet hoses, allowing continuous circulation of oil.

Forming parameters were selected based on preliminary trials and literature recommendations to ensure stable deformation: vertical step size $t_z$= 1.0 mm, spindle speed $S$=2400 rpm, tool feed rate F=1000 mm/min, and tool diameter D=6 mm. The NC program generated for the numerical simulation was directly transferred to the CNC machine, ensuring full consistency between simulation and experiment.

### 3.3. THICKNESS MEASUREMENT METHODOLOGY

Thickness distribution was evaluated using a systematic and repeatable measurement procedure. After forming, each truncated quadrilateral component was sectioned along a generatrix of the inclined wall. Nineteen measurement points were marked at intervals of 10 mm along the wall, covering both the upper corner region and the bottom transition zone. Thickness measurements were performed using a digital micrometer, with three repeated readings taken at each location to minimize measurement uncertainty (Figure 6a).

Process stability was examined through the repeatability and verification of dimensional consistency in the formed geometry. The present validation is based on a single representative specimen; while measurement repeatability was ensured, broader statistical generalization would benefit from multiple specimens. This aspect will be addressed in future work through an expanded experimental campaign incorporating statistical averaging.

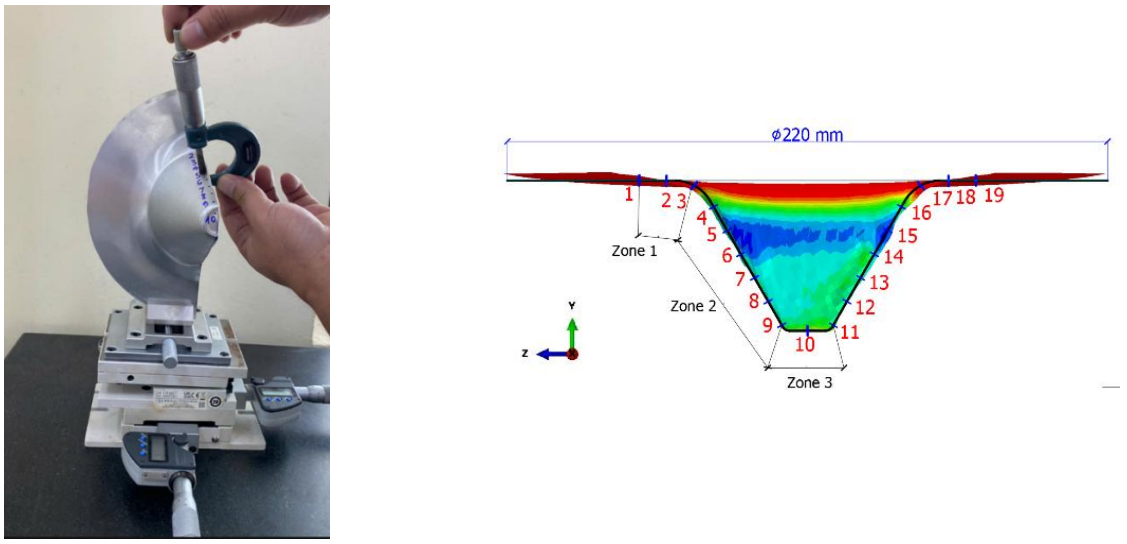


a) b)

Fig. 6. Thickness measurement procedure for the truncated quadrilateral component: (a) formed specimen with predefined measurement locations; (b) corresponding spatial distribution of numerical sampling points extracted from the finite element model

In parallel, numerical thickness data were extracted from the FE model at nodes corresponding to the experimental measurement locations (Fig. 6b). This one-to-one correspondence between experimental and numerical data points enables a rigorous quantitative comparison of thickness evolution along the wall. The combined use of experimental measurements and FE-based thickness extraction provides a robust basis for validating the proposed HA-SPIF modelling framework and for assessing the influence of hydraulic pressure and material anisotropy on thinning behaviour.

## 4. RESULTS AND DISCUSSION

### 4.1. INFLUENCE OF HARDENING REPRESENTATION ON THICKNESS DISTRIBUTION OF TRUNCATED SQUARE PYRAMID IN HA-SPIF SIMULATIONS

To accurately describe the plastic response of AA1050 under HA-SPIF conditions, the Voce hardening law was calibrated using uniaxial tensile data obtained along three material orientations: rolling direction (RD, 0°), 45° to RD, and transverse direction (TD, 90°). A systematic comparison between finite element predictions and experimentally measured thickness profiles was subsequently performed to determine the most representative material calibration for further simulations.

Unless otherwise stated, the following parameters were kept constant within this subsection: hydraulic pressure $P$ = 0 bar, vertical step size $t_z$ = 1.0 mm, tool feed rate $F$ = 1000 mm/min, spindle speed $S$ = 2400 rpm, and tool diameter $D$ = 6 mm.

The deviation between simulated and experimental thickness values was quantified using Equation (2):

$$\Delta t_b(\%) = (\left|t_{b-E} \quad - t_{b-S}\right|)/t_{b-E} \tag{2}$$

where $t_{b-S}$ and $t_{b-E}$ denote the wall thickness obtained from simulation and experiment, respectively.

In the numerical model, thickness values were extracted along nodal paths from the center to the inclined wall of the truncated pyramid. Correspondingly, in the experimental investigation, wall thickness was measured at 19 equally spaced locations (18 intervals of 10 mm) along the generatrix of the inclined surface. To ensure consistency, only half of the cross-section was considered in Fig. 7a due to geometric symmetry.

The thickness profile along the wall height can be divided into three characteristic deformation regions, symmetric about the mid-plane of the component (Fig. 6b). The first region (Points 1–3 and 17–19) corresponds to the initial bending-dominated stage, where thickness variation remains limited. The second region (Points 4–9 and 11–16) is governed by combined shear and tensile stretching; this zone exhibits the most significant thinning and therefore represents the critical region with respect to fracture initiation. The third region (Point 10), located near the bottom transition, undergoes minimal plastic deformation, and the measured thickness remains close to the initial sheet value.

As shown in Fig. 7f, both numerical and experimental results consistently indicate that Point 5, located within the tensile–shear deformation zone, exhibits the minimum wall

thickness. Experimentally, the minimum thickness was measured as $t_{b-E}$= 0.425 mm. The corresponding simulated values were 0.438 mm for the 0° model, 0.393 mm for the 45° model, and 0.364 mm for the 90° model. The maximum local deviation reached 14.35% for the 90° model at Point 5, followed by 7.53% for the 45° model, whereas the 0° model exhibited a markedly lower deviation of only 3.51% (observed at Point 15).

When considering the average deviation across all measurement points, the Voce model calibrated along the rolling direction (0°) yielded the smallest mean error of 1.56%, compared to 4.23% and 6.01% for the 45° and 90° orientations, respectively. These results clearly demonstrate that the Voce hardening model identified along the rolling direction provides the most reliable representation of the deformation behavior of AA1050 under HS-SPIF conditions.

Accordingly, the Voce hardening law calibrated in the rolling direction (0°) was adopted for all subsequent numerical analyses. This rigorous validation not only justifies the material model selection but also explains why the largest discrepancies are consistently observed in the shear–stretching zone, where material anisotropy and strain localization are most pronounced. The validated framework thus establishes a robust and physically sound basis for the subsequent parametric investigations and optimization studies.

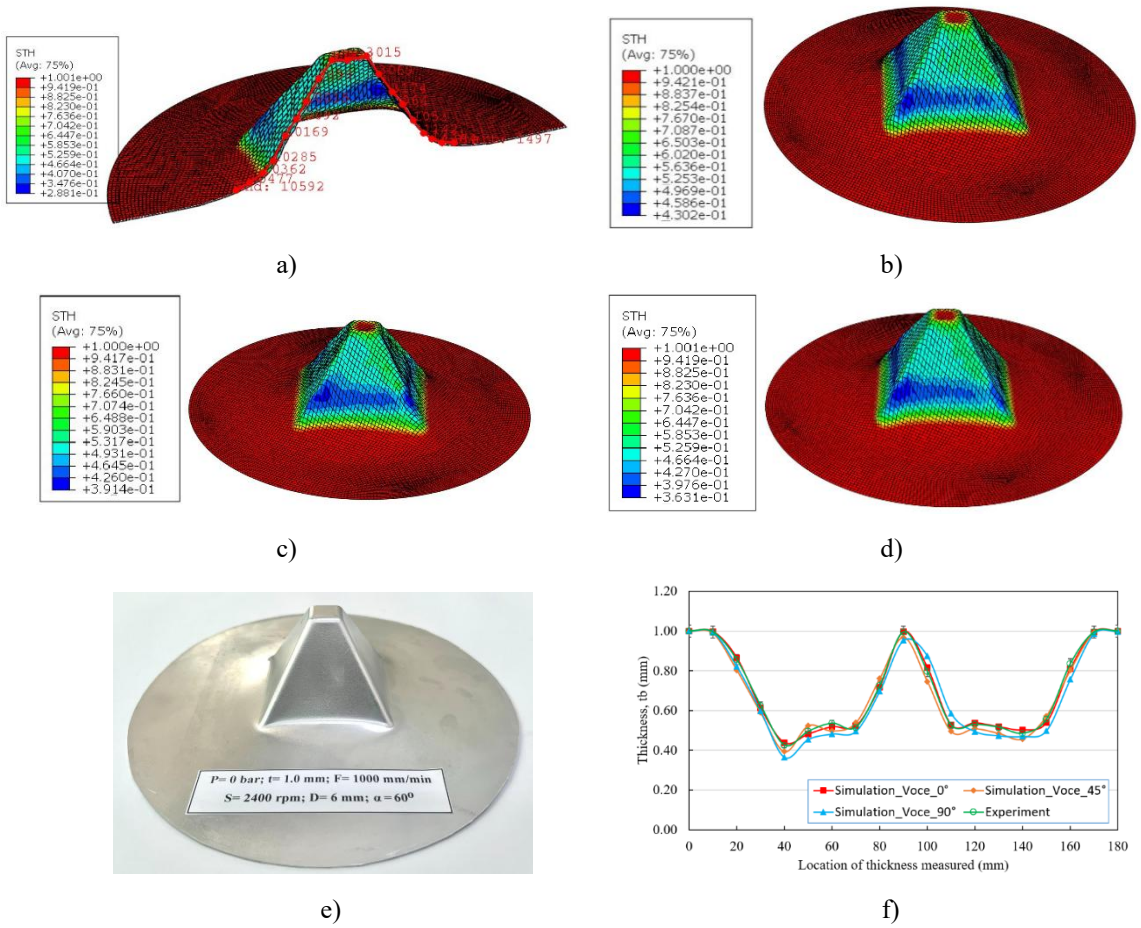


Fig. 7. Numerical prediction and experimental validation of wall thickness distribution in the truncated square pyramid: a) schematic cross-sectional representation; finite element results using Voce hardening calibrated along b) 0° (RD), c) 45° to RD, and d) 90° (TD); e) experimental thickness measurements; and f) comparison between numerical and experimental thickness profiles, indicating the bending-dominated, shear–stretching, and bottom regions

### 4.2. EFFECT OF HYDRAULIC PRESSURE ON WALL THICKNESS DISTRIBUTION IN HS-SPIF

To investigate the influence of hydraulic support pressure $P$ on wall thickness evolution during HS-SPIF, four pressure levels were examined: 0 bar, 0.1 bar, 0.2 bar, and 0.3 bar. Unless otherwise specified, the process parameters were kept constant in this subsection: tool feed rate $F$ = 1000 mm/min, vertical step size $t_z$=1.0 mm, and tool diameter $D$ = 6 mm. Figure 8 (a-d) presents the simulated deformed shapes under each pressure condition, while the corresponding thickness distributions along the inclined wall are summarized in Fig. 8e.

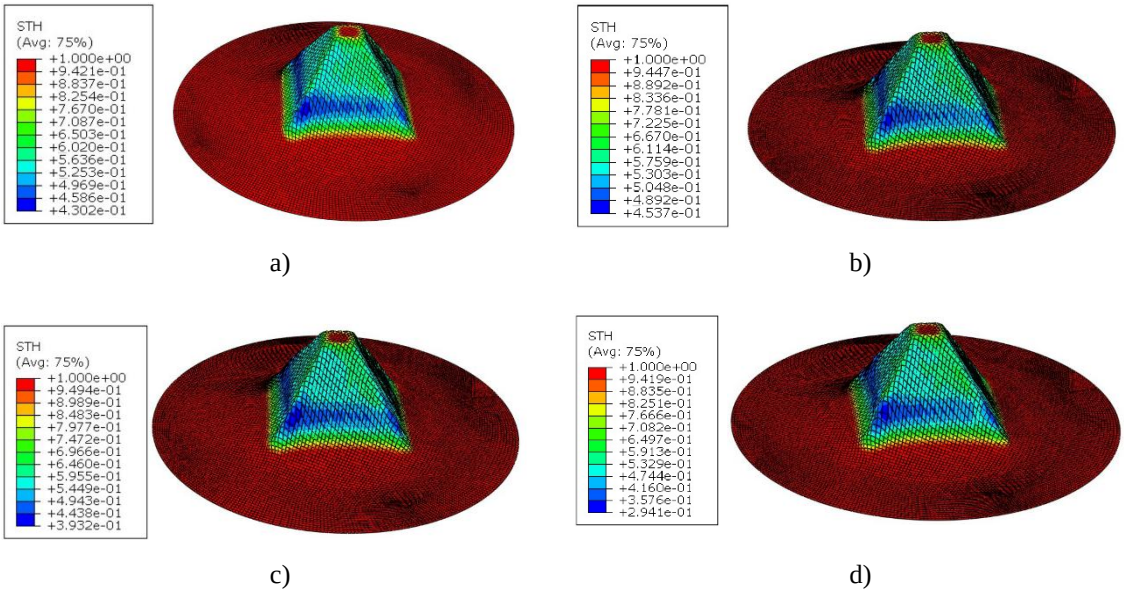


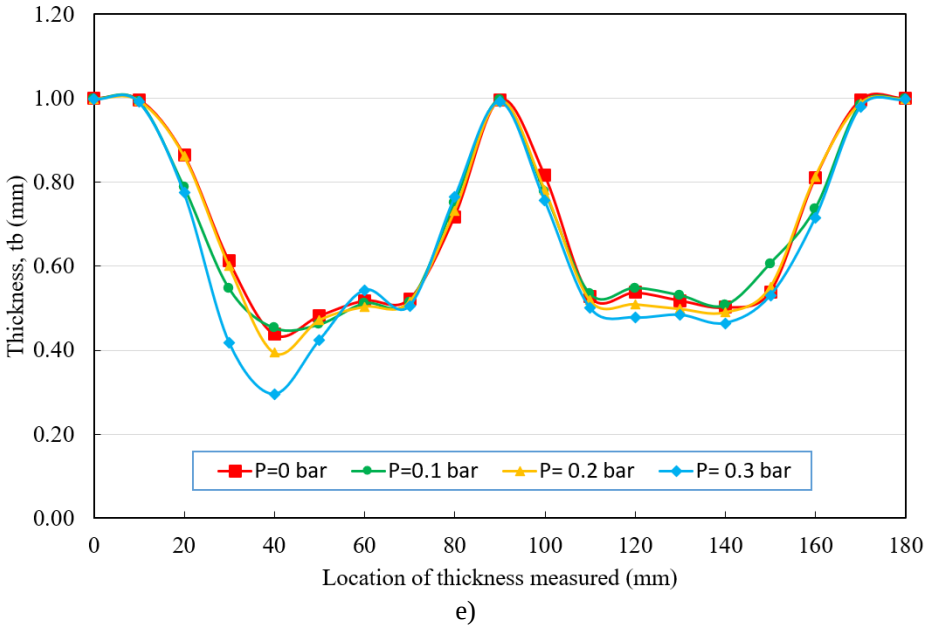


Fig. 8. FEM-predicted deformation and wall thickness distribution under varying hydraulic pressures: a) $P$ = 0 bar; b) $P$ = 0.1 bar; c) $P$ = 0.2 bar; d) $P$ = 0.3 bar; e) comparison of wall thickness along the inclined surface

The results indicate that wall thickness at measurement locations 1, 2, 10, 18, and 19 remains relatively insensitive to variations in hydraulic pressure. In contrast, significant thinning is consistently observed at Point 5, located within the tensile–shear deformation zone. Without hydraulic pressure (P = 0 bar), the minimum thickness was predicted to be 0.438 mm. Introducing a moderate pressure of 0.1 bar resulted in a noticeable thickening effect, increasing the minimum thickness to 0.462 mm. However, further increasing the pressure to 0.2 bar led to enhanced thinning, with a minimum thickness of 0.394 mm, while a pressure of 0.3 bar caused severe thinning, reducing the minimum thickness to 0.295 mm. These findings reveal a non-monotonic influence of hydraulic pressure on wall thickness evolution. Moderate hydraulic support effectively suppresses excessive stretching by providing counter-pressure, thereby improving thickness uniformity. Conversely, excessive pressure intensifies local contact stresses and material flow instability, leading to pronounced thinning. Based on this comprehensive analysis, a hydraulic pressure of 0.1 bar is identified as the optimal condition for HS-SPIF of truncated square pyramid geometries.

### 4.3. EFFECT OF TOOL FEED RATE ON WALL THICKNESS IN HA-SPIF

The influence of tool feed rate $F$ on wall thickness distribution was investigated by considering five feed rates: 500, 750, 1000, 1250, and 1500 mm/min. Throughout this subsection, hydraulic pressure was maintained at $P$ = 0.1 bar, while the vertical step size and tool diameter were fixed at $t_z$ = 1.0 mm and $D$ = 6 mm, respectively. The simulated deformed configurations corresponding to each feed rate are presented in Figs 9(a–e), and the resulting thickness distributions along the inclined wall are compared in Fig. 9(f).

Across all cases, thickness at positions 1, 2, 10, 18, and 19 exhibits minimal variation. However, significant thinning occurs in the tensile–shear deformation zone, particularly at Point 5. At a feed rate of 500 mm/min, the minimum thickness was predicted as 0.432 mm. Increasing the feed rate to 750 mm/min led to a pronounced improvement in thickness uniformity, with a minimum thickness of 0.487 mm. Beyond this value, further increases in feed rate resulted in progressive thinning, with minimum thicknesses of 0.462 mm, 0.406 mm, and 0.339 mm at feed rates of 1000, 1250, and 1500 mm/min, respectively.

This behaviour can be attributed to the competing effects of strain rate sensitivity and localized deformation. Moderate feed rates promote more stable material flow, whereas excessive feed rates intensify localized stretching and reduce thickness uniformity. Consequently, a feed rate of 750 mm/min is identified as the most favourable condition for HS-SPIF under the investigated parameters.

### 4.4. EFFECT OF VERTICAL STEP SIZE ON WALL THICKNESS IN HA-SPIF

To assess the effect of vertical step size ($t_z$) on wall thickness evolution, five values were examined: 0.25, 0.50, 1.0, 1.5, and 2.0 mm. In this subsection, hydraulic pressure and tool feed rate were kept constant at P = 0.1 bar and $F$ = 1000 mm/min, respectively, while the tool diameter was fixed at D = 6 mm.

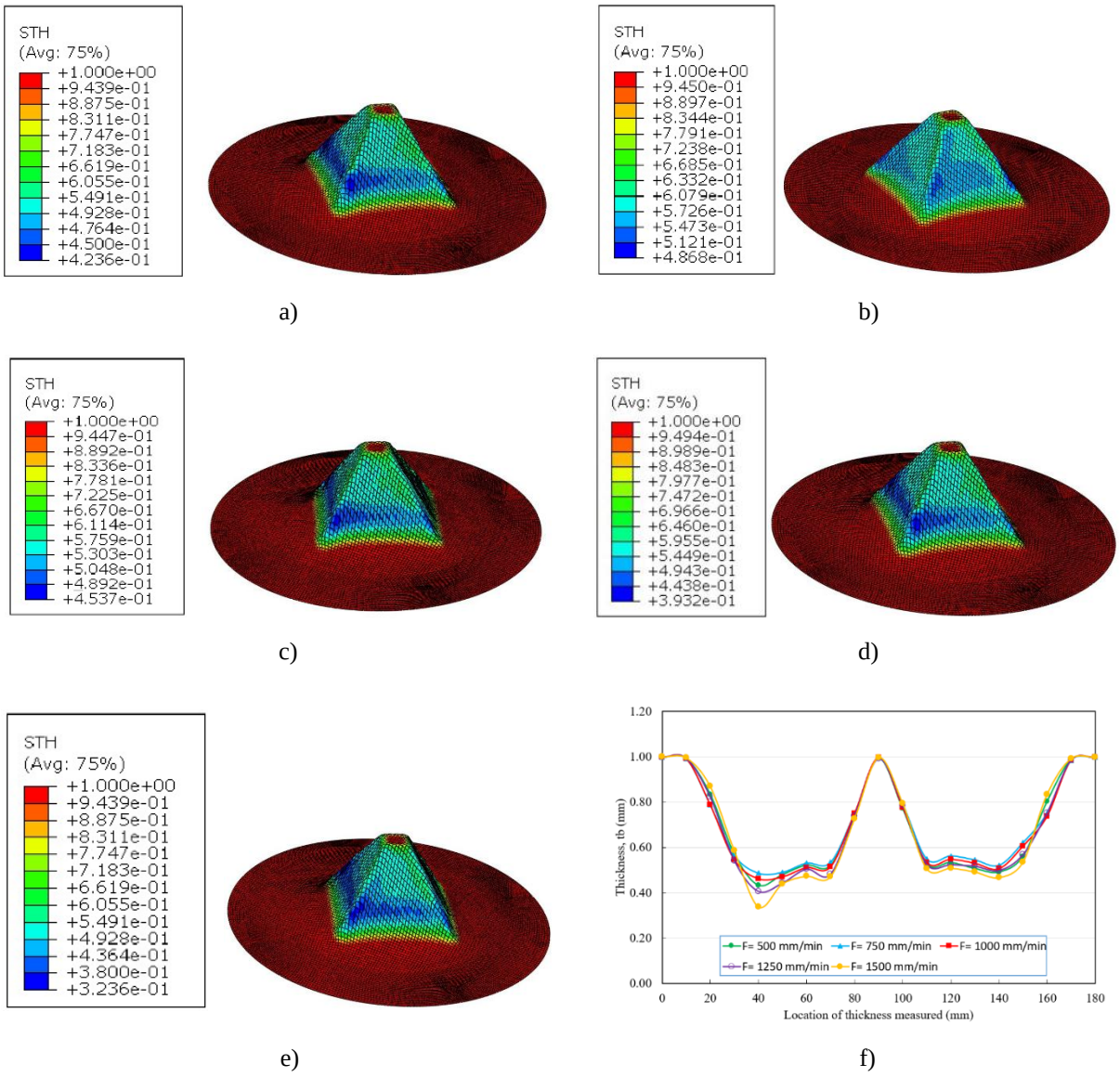


Fig. 9. FEM-predicted deformation and wall thickness distribution at varying tool feed rates: a) $F$ = 500 mm/min; b) $F$ = 750 mm/min; c) $F$ = 1000 mm/min; d) $F$ = 1250 mm/min; e) $F$ = 1500 mm/min; (f) comparison of wall thickness along the inclined surface

The simulated deformed geometries corresponding to each step size are presented in Figs 10(a–e), and the associated thickness distributions along the inclined wall are compared in Fig. 10(f). The results indicate that step size has a pronounced effect on wall thickness evolution, particularly in the tensile–shear zone. While thickness remains relatively stable at positions 1, 2, 10, 18, and 19, the minimum thickness at Point 5 varies significantly with step size. Specifically, the minimum thicknesses were 0.398 mm ($t_z$= 0.25 mm), 0.493 mm ($t_z$= 0.50 mm), 0.462 mm ($t_z$= 1.0 mm), 0.386 mm ($t_z$= 1.5 mm), and 0.272 mm ($t_z$= 2.0 mm).

These results highlight that excessively small or large step sizes adversely affect thickness uniformity. A moderate step size of 0.50 mm achieves the most favourable balance between deformation stability and thickness preservation, thereby minimizing excessive thinning.

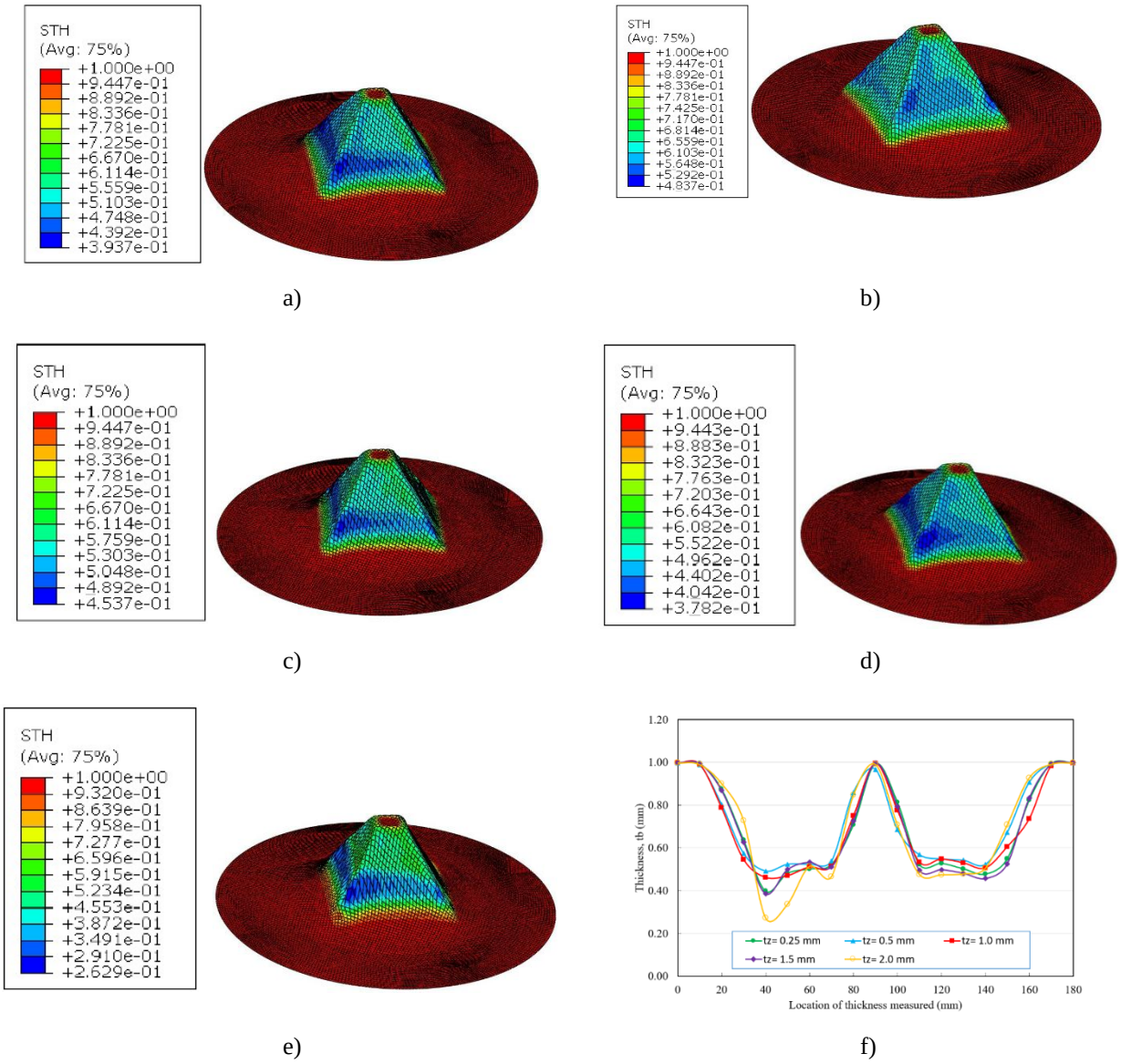


Fig. 10. FEM-predicted deformation and wall thickness distribution for varying vertical step sizes: a) $t_z$= 0.25 mm; b) $t_z$= 0.50 mm; c) $t_z$= 1.0 mm; d) $t_z$= 1.5 mm; e) $t_z$= 2.0 mm; f) comparison of wall thickness along the inclined surface

### 4.5. EXPERIMENTAL VALIDATION USING OPTIMIZED PROCESS PARAMETERS

Based on the comprehensive parametric analyses, the optimal HA-SPIF parameters were identified as $P$ = 0.1 bar, $F$ = 750 mm/min, and $t_z$= 0.5 mm. These parameters were applied consistently in both the numerical simulation and the experimental validation presented in this subsection. The predicted thickness distribution under the optimized condition is shown in Fig. 11(a), with a minimum wall thickness of 0.526 mm. The corresponding experimentally formed component (Fig. 11(b)) exhibited a minimum thickness of 0.515 mm. A direct comparison of thickness values at all predefined measurement locations is provided in Fig. 11(c).

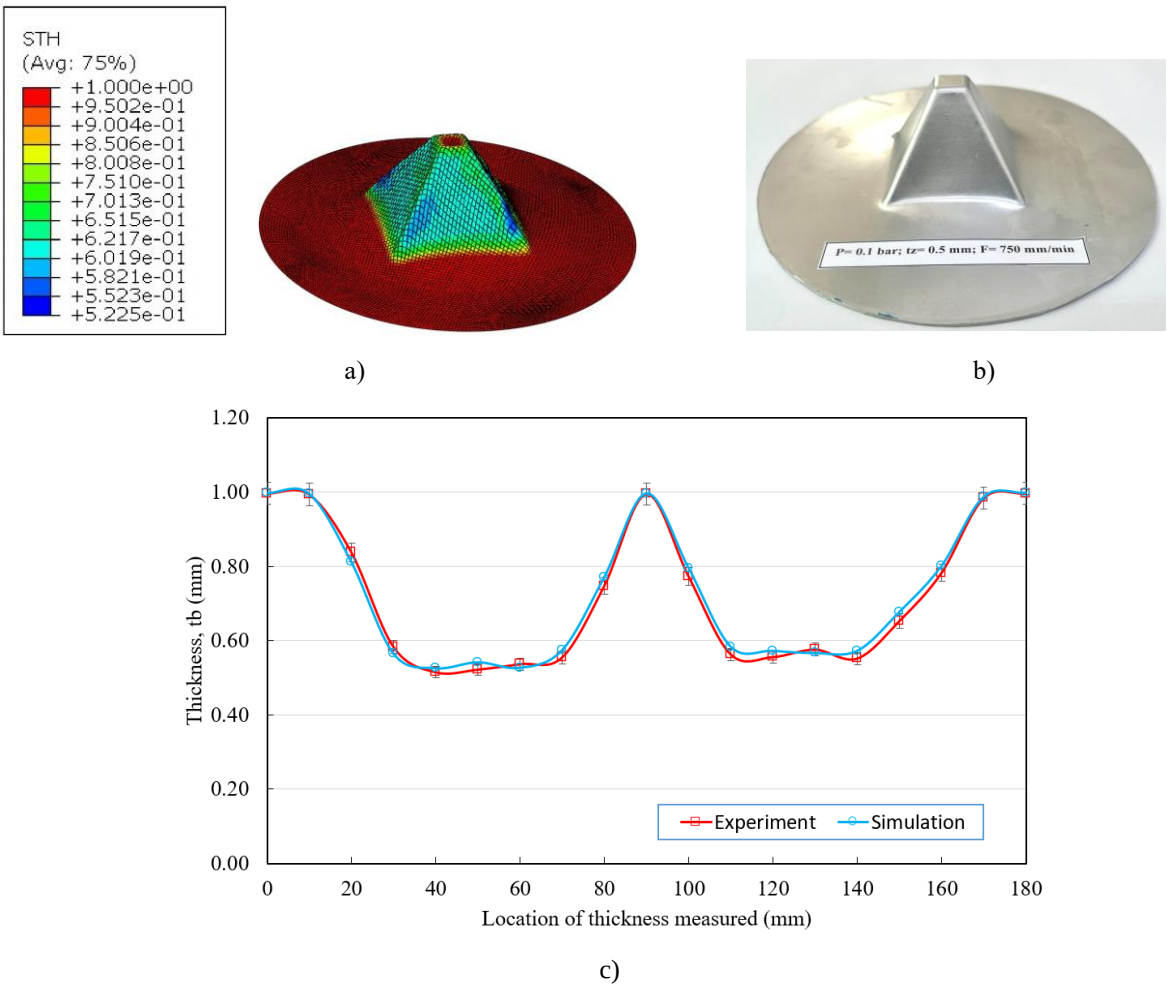


Fig. 11. Comparison of wall thickness in the truncated square pyramid using optimized HS-SPIF parameters: a) FEM-predicted distribution; b) experimentally formed part; c) thickness distribution comparison between simulation and experiment

The average deviation between numerical and experimental thickness values was calculated to be only 1.09%, demonstrating excellent agreement. This high level of consistency confirms the robustness of the proposed FE modelling framework and validates the effectiveness of hydraulic support in enhancing thickness uniformity and formability in HA-SPIF.

## 4. CONCLUSIONS

This study comprehensively investigated the effects of rolling direction and hydraulic pressure on wall thickness distribution during SPIF of AA1050 aluminum sheets. By integrating experimental testing and FE simulation, and employing an anisotropic Voce hardening model calibrated along different rolling directions, the research elucidated the material behaviour under hydraulically assisted forming conditions. The key findings and contributions are summarized as follows:

- The calibrated anisotropic constitutive model reproduced the measured thickness trends with good accuracy along the rolling direction (0°), demonstrating reliable predictive capability within the investigated parameter range. The results confirm that incorporating directional hardening behaviour is essential for capturing localized thinning in non-axisymmetric geometries.
- Hydraulic pressure significantly influenced wall thickness distribution and localized thinning. Position 5 exhibited the most pronounced thinning, while other regions maintained relatively stable thickness. An applied hydraulic pressure of 0.1 bar was identified as optimal for ensuring uniform wall thickness and mitigating excessive thinning in truncated square pyramid components.
- Wall thickness at positions 1, 2, 10, 18, and 19 remained largely unaffected by variations in tool feed rate and vertical step size, whereas region 2, particularly position 5, experienced thinning due to tensile deformation. The optimal tool feed rate and vertical step size were determined as 750 mm/min and 0.50 mm, respectively, to enhance wall thickness uniformity and minimize thinning during HS-SPIF.
- Validation with optimized parameters ($P$ = 0.1 bar, $F$ = 750 mm/min, $t_z$= 0.5 mm) showed excellent agreement between FE simulation and experimental results, with minimum wall thickness values of 0.526 mm (simulation) and 0.515 mm (experiment), yielding an average deviation of only 1.09%. This confirms the reliability of the proposed simulation framework for predictive and process optimization purposes.

This study emphasizes the critical roles of rolling direction, hydraulic pressure, and process parameter selection in achieving superior formability in SPIF. The methodology presented here can be extended to other lightweight alloys for precision forming applications. The findings contribute to a deeper understanding of material deformation behaviour in incremental forming and provide a solid foundation for developing advanced hydraulic-assisted metal forming strategies.

## ACKNOWLEDGEMENTS

*This research is funded by Hanoi University of Science and Technology (HUST) under Grant No. T2024-PC-028*

## REFERENCES

[1] GATEA S., LU B., CHEN J., OU H., MCCARTNEY G., 2019, *Investigation of the Effect of Forming Parameters in Incremental Sheet Forming Using a Micromechanics Based Damage Model*, Int. J. Mater. Form., 12/4, 553–574, https://doi.org/10.1007/s12289-018-1434-3.

[2] KUMAR A., GULATI V., KUMAR P., SINGH V., KUMAR B., SINGH H., 2019, *Parametric Effects on Formability of AA2024-O Aluminum Alloy Sheets in Single Point Incremental Forming*, J. Mater. Res. Technol., 8/1, 1461–1469, https://doi.org/10.1016/j.jmrt.2018.11.001.

[3] HOANG T.K., LUYEN T.T., NGUYEN D.T., 2023, *Enhancing/Improving Forming Limit Curve and Fracture Height Predictions in the Single-Point Incremental Forming of Al1050 Sheet Material*, Materials (Basel)., 16/23, 1–19, 2023, https://doi.org/10.3390/ma16237266.

[4] ABDELHAFEEZ HASSAN A., KÜÇÜKTÜRK G., YAZGIN H.V., GÜRÜN H., KAYA D., 2022, *Selection of Constitutive Material Model for the Finite Element Simulation of Pressure-Assisted Single-Point Incremental Forming*, Machines, 10/10, https://doi.org/10.3390/machines10100941.

[5] FATEMI A., MOLLAEI DARIANI B., 2024, *A Novel Experimental Method for Determination of Forming Limits With Generalized Non-Planar Stress State Using Hydro-Assisted Incremental Forming*, Discov. Mech. Eng., 3/1, https://doi.org/10.1007/s44245-024-00048-5.

[6] SHANG M., YANG Y.LI,M., CHEN Y., BAI L., LI P., 2023, *Wall Thickness Uniformity in ISF of Hydraulic Support: System Design, Finite Element Analysis and Experimental Verification*, Machines, 11/3, https://doi.org/10.3390/machines11030353.

[7] LUYEN T.T., HOANG T.K., NGUYEN D.T., 2024, *A Combined Simulation and Experimental Investigation on Tool Radius Infuence on Enhancing the Formability SPIF Process for Al1050 Sheet Material*, International Journal of Modern Physics B, 2540024, https://doi.org/10.1142/S0217979225400247.

[8] HOANG T.-K., LUYEN T.-T., NGUYEN D.-T., 2025, *An In-Depth Analysis of Process Parameter Effects on Forming Forces in Single Point Incremental Forming of Al1050 Aluminium Sheets*, Adv. Mater. Process. Technol., 1/14.

[9] NGUYEN D.-T., MAC T.-B., HOANG T.-K., NGUYEN T.-H., 2026, *Integrated Experimental–Numerical Analysis and Optimization of Wall Thickness in Single Point Incremental Forming of AA1050 Aluminum Alloy*, J. Brazilian Soc. Mech. Sci. Eng., 48/1, 56.

[10] HOANG T.-K., MAC T.-B., LUYEN T.-T., NGUYEN D.-T., 2025, *Parametric Study and Multi-Objective Optimization in Heat-Assisted Single Point Incremental Forming of AA1050 Aluminum Alloy Using Experimental Design Methods*, Int. J. Adv. Manuf. Technol., 1–22.

[11] HOANG T.-K., MAC T.-B., LUYEN T.-T., PHAM Q.-T., NGUYEN D.-T., 2025, *Integrated Experimental Study on Thickness Uniformity, Thinning Limit, and Forming Force in Heat-Assisted Single-Point Incremental Forming Of AA1050 Aluminum Alloy*, J. Mater. Eng. Perform., 1–17.

[12] LUYEN T.-T., MAC T.-B., HOANG T.-K., NGUYEN D.-T., 2025, *A Study on Improving Thickness Uniformity And Geometric Precision of Truncated Cone Components in Hydraulic Pressure-Assisted Single Point Incremental Forming*, J. Manuf. Process., 152, 488–505, https://doi.org/10.1016/j.jmapro.2025.08.020.

[13] HIBBITT, KARLSSON & SORENSEN Inc, 2001, *ABAQUS / CAE User's Manual*, Ver. 6.10.1.